ELSEVIER International Journal of Mass Spectrometry and Ion Processes 141 (1995) 101–116

International Journal of Mass Spectrometry and Ion Processes

Frequency shifts and modulation effects due to solenoidal magnetic field inhomogeneities in ion cyclotron mass spectrometry

Dale W. Mitchell, Alan L. Rockwood, Richard D. Smith*

Pacific Northwest Laboratory, Chemical Sciences Department, P.O. Box 999, P8-19, Richland, WA 99352, USA

Received 23 May 1994; accepted 12 October 1994

Abstract

Solenoidal (i.e. axially symmetric) magnetic field inhomogeneities, which in addition have symmetry under the operation $z \rightarrow -z$ are the most important to Fourier transform-ion cyclotron resonance (FT-ICR) mass spectrometry since they introduce frequency shifts at first-order in perturbation theory. Frequency shifts for all three fundamental modes are derived for the leading second-order and fourth-order solenoidal inhomogeneities without any restrictions on the initial conditions. The analytical frequency shifts agree very well with frequency shifts obtained from numerical trajectory calculations using the exact classical equations of motion. The effect of the inhomogeneity on the ion trajectory is solved analytically. For a strong magnetic bottle field, the cyclotron motion is frequency modulated at twice the z-oscillation frequency resulting in sidebands. However, the amplitude of these sidebands is negligibly small for typical inhomogeneity strengths. The effect of a magnetized ICR trap on the homogeneity of the magnetic field is studied by analytical methods. We find that the leading magnetic bottle field decreases as d^{-3}, where d is the cylindrical ion trap diameter.

Keywords: Fourier transform ion cyclotron resonance mass spectrometry; Frequency shifts; Ion dynamics; Magnetic field inhomogeneities; Magnetic materials

1. Introduction

The most important feature of a Fourier transform-ion cyclotron resonance (FT-ICR) mass spectrometer [1,2] is a strong magnetic field $\vec{B}_0$ directed along the z-axis of a configuration of electrodes that comprise the ICR trap. Recently, we have studied the effects of non-quadrupolar electrostatic trapping potentials [3–5] and non-linear excitation electric fields [6] on ion motion. In this work, we investigate the effects of magnetic field inhomogeneities on the dynamics of a single ion in an ICR trap.

Neglecting the trapping potential and assuming that $\vec{B}_0$ is homogeneous, an ion of mass m and charge q has a fundamental periodic motion perpendicular to B_0 at the cyclotron frequency

$$\omega_c = qB_0/m \tag{1}$$

from which a mass spectrum is obtained [1]. Unfortunately, due to imperfect shimming of the finite length solenoid magnet and/or magnetization of the ICR trap and its support

* Corresponding author.

SSDI 0168-1176(94)04106-7

structure, magnetic field inhomogeneities are present which perturb the ion's motion leading to position-dependent frequency shifts and possibly modulation effects. In most FT-ICR experiments the existence of position-dependent frequency shifts is undesirable since they can degrade mass resolution, precision and experimental reproducibility. However, in some applications the intentional addition of a strong inhomogeneous magnetic field in the form of a magnetic bottle is crucial to the success of precision measurements of the g value of the electron and positron [7], as well as the recently proposed [8] combination of magnetic resonance spectroscopy with FT-ICR detection. A magnetic bottle is a particular type of magnetic field whose dependence along the z-axis is quadratic in z-position. The leading inhomogeneity term for all solenoidal (i.e. axially symmetric) magnetic fields, which in addition possess symmetry under the operation $z \rightarrow -z$, is in the form of a magnetic bottle.

Schuch et al. [9] have derived the cyclotron frequency shift due to the leading radial magnetic field component of a finite length solenoid by a quantum mechanical minimized wave packet approach [10] and found that this shift is negligibly small. Laukien [11], using classical mechanics and the guiding center approximation, has calculated the cyclotron frequency shift (in the limit of zero magnetron and z-axis oscillation) due to gradients of the axial magnetic field component, demonstrating that radial gradients are the most important to the cyclotron frequency shift. Employing quantum mechanical perturbation theory, Brown and Gabrielse [7] have derived the first-order energy correction due to the presence of a magnetic bottle from which frequency shifts can be obtained.

Our work differs from these earlier investigations in several important respects. Since most FT-ICR experiments make measurements on ions with large quantum numbers, the ion motion is nearly classical. The frequency shifts are derived by first-order classical perturbation theory without any restriction on initial conditions [12]. Next, while previous studies have concentrated on frequency shifts due to only the lowest-order inhomogeneity, i.e. the second-order magnetic bottle field, we present analytical results for second- and fourth-order inhomogeneities. We shall demonstrate that for the relatively large mode-amplitudes encountered in FT-ICR, the fourth-order inhomogeneity gives a substantial contribution to the frequency shifts which can be on the order of or greater than the contribution due to the second-order term. These analytical frequency shifts agree well with exact numerical results. The influence of the magnetic bottle term on the ion trajectory is also derived analytically by an approximate perturbative method. Finally, magnetic field inhomogeneities due to the magnetization of the ICR trap and its support structure are examined by modeling the apparatus as infinitesimal rings of uniform magnetization [7].

2. Procedure

In the quadrupole approximation [7,12–14] which we consider as the unperturbed motion, the ion moves in a quadrupolar electrostatic potential Φ_0 whose z-axis is aligned parallel to a constant homogeneous magnetic field $B_0\hat{k}$. The unperturbed Hamiltonian is

$$H_0 = \frac{1}{2m}(\vec{P} - q\vec{A}_0)^2 + q\Phi_0 \tag{2}$$

where $\vec{P}$ is the canonical momentum, and $\vec{A}_0$ is the vector potential due to the unperturbed magnetic field given by

$$\vec{A}_0 = \tfrac{1}{2}B_0(-y\hat{i} + x\hat{j}) = \tfrac{1}{2}\rho B_0\hat{\theta} \tag{3}$$

where the first equality on the right is the Cartesian coordinate representation while the second is the cylindrical coordinate representation ($\rho^2 = x^2 + y^2$) of the unperturbed vector

potential. The quadrupole (trapping) potential, in cylindrical coordinates (ρ, z, θ), is

$$\Phi_0(\rho, z) = V_t \frac{D_2}{d^2}\left(z^2 - \frac{1}{2}\rho^2\right) \tag{4}$$

where V_t is the applied potential on the trap plates with ground on all others, d is the ICR trap width and D_2 is a dimensionless, geometry-dependent coefficient. For example, $D_2 = 2.7737$ for a cubic trap and $D_2 = 2.8404$ for a cylindrical trap whose length and diameter are equal. A constant term in the electrostatic potential has been neglected in Eq. (4) since this constant potential does not contribute to the dynamics. Putting Eqs. (3) and (4) in Eq. (2), the quadrupolar Hamiltonian, H_0, can be written in Cartesian coordinates as

$$\begin{aligned} H_0 = {} & \frac{1}{2m}(P_x^2 + P_y^2 + P_z^2) \\ & + \tfrac{1}{2}(\omega_{+0} + \omega_{-0})(P_x y - P_y x) \\ & + \frac{m}{8}(\omega_{+0} - \omega_{-0})^2(x^2 + y^2) + \frac{m}{2}\omega_{z0}^2 z^2 \end{aligned} \tag{5}$$

The solution of the classical equations of motion is well known [12,14]

$$\begin{aligned} x(t) &= R_+ \cos\phi_+ + R_- \cos\phi_- \\ y(t) &= -R_+ \sin\phi_+ - R_- \sin\phi_- \\ z(t) &= A_z \cos\phi_z \end{aligned} \tag{6}$$

where

$$\begin{aligned} \phi_+ &= \omega_{+0} t + \beta_+ \\ \phi_- &= \omega_{-0} t + \beta_- \\ \phi_z &= \omega_{z0} t + \beta_z \end{aligned} \tag{7}$$

and R_+, R_- and A_z are the cyclotron radius, magnetron radius, and z-oscillation amplitude, respectively, which are constants of motion (as are their corresponding phases β_+, β_-, and β_z) for the quadrupole approximation. The unperturbed eigenfrequencies are

$$\begin{aligned} \omega_{+0} &= \frac{\omega_c}{2} + \frac{\omega_c}{2}\sqrt{1 - \frac{2\omega_{z0}^2}{\omega_z^2}} \\ \omega_{-0} &= \frac{\omega_c}{2} - \frac{\omega_c}{2}\sqrt{1 - \frac{2\omega_{z0}^2}{\omega_c^2}} \\ \omega_{z0} &= \sqrt{\frac{2qV_t D_2}{md^2}} \end{aligned} \tag{8}$$

The ion motion is a linear superposition of three simple harmonic oscillators: cyclotron motion at frequency ω_{+0} and magnetron motion at frequency ω_{-0} in the x–y plane, and a z-oscillation along the z-axis at frequency ω_{z0}. Under most conditions one has the hierarchy of frequencies $\omega_{+0} \approx \omega_c \gg \omega_{z0} \gg \omega_{-0}$. For simplicity, we assume here that this hierarchy is valid.

Thus far, only the unperturbed motion has been discussed. In order to solve the perturbed problem, with a Hamiltonian $H = H_0 + \Delta H$, where ΔH is the perturbation, it is convenient to make a canonical transformation from Cartesian coordinates to action-angle (J_j, Q_j) given by [12,13]

$$\begin{aligned} x &= \sqrt{\frac{2}{m\omega_p}}(\sqrt{J_1}\cos Q_1 + \sqrt{J_2}\cos Q_2) \\ y &= \sqrt{\frac{2}{m\omega_p}}(-\sqrt{J_1}\sin Q_1 + \sqrt{J_2}\sin Q_2) \\ z &= \sqrt{\frac{2J_3}{m\omega_{z0}}}\cos Q_3 \\ P_x &= \sqrt{\frac{m\omega_p}{2}}(-\sqrt{J_1}\sin Q_1 - \sqrt{J_2}\sin Q_2) \\ P_y &= \sqrt{\frac{m\omega_p}{2}}(-\sqrt{J_1}\cos Q_1 + \sqrt{J_2}\cos Q_2) \\ P_z &= -\sqrt{2J_3 m\omega_{z0}}\sin Q_3 \end{aligned} \tag{9}$$

where

$$\omega_p = \omega_{+0} - \omega_{-0} \tag{10}$$

Also, J_1, J_2 and J_3 are the action variables of the cyclotron, magnetron and z-oscillation modes, respectively, and Q_j are the corresponding angle variables. Comparing Eq. (9) with Eq. (6) demonstrates that the action variables J_j are proportional to the squares of the mode amplitudes, $Q_1 = \phi_+$, $Q_3 = \phi_z$, and $Q_2 = -\phi_-$. The angle variable for the magnetron mode, Q_2, is negative of the magnetron phase, $\phi_- = \omega_{-0}t + \beta_-$, in this formulation indicating that while the cyclotron and z-oscillation angle variables (Q_1 and Q_3, respectively) rotate with the same phase as the ion, the magnetron angle variable rotates exactly opposite the magnetron motion. This is a consequence of the particular choice of canonical transformation employed, Eq. (9). It is possible to derive a canonical transformation which has Q_2 rotating with the same phase sense as the magnetron motion [13]. However, the final results for the ion's dynamics are independent of the transformation employed. Using Eq. (9), the Hamiltonian H transforms to

$$H = \omega_{+0}J_1 - \omega_{-0}J_2 + \omega_{z0}J_3 + \Delta H(J_j, Q_j) \tag{11}$$

The equations of motion evaluated from Hamilton's equations are

$$\begin{aligned} \dot{J}_j &= -\frac{\partial \Delta H}{\partial Q_j} \\ \dot{Q}_1 &= \omega_{+0} + \frac{\partial \Delta H}{\partial J_1} \\ \dot{Q}_2 &= -\omega_{-0} + \frac{\partial \Delta H}{\partial J_2} \\ \dot{Q}_3 &= \omega_{z0} + \frac{\partial \Delta H}{\partial J_3} \end{aligned} \tag{12}$$

A first-order approximation to Eq. (12) can be obtained by averaging over the angle variables, Q_j. Equivalently, and with less computational effort, the perturbation Hamiltonian $\Delta H(J_j, Q_j)$ can be averaged over the angle variables to yield $\langle \Delta H(J_j) \rangle$, which leads to the first-order approximation

$$\begin{aligned} \dot{J}_j &\cong 0 \\ \dot{Q}_1 &\cong \omega_{+0} + \frac{\partial \langle \Delta H \rangle}{\partial J_1} \\ \dot{Q}_2 &\cong -\omega_{-0} + \frac{\partial \langle \Delta H \rangle}{\partial J_2} \\ \dot{Q}_3 &\cong \omega_{z0} + \frac{\partial \langle \Delta H \rangle}{\partial J_3} \end{aligned} \tag{13}$$

where the brackets $\langle\ \rangle$ denote the average over the angle variables. These expressions are valid provided that there are no phase terms with commensurate frequencies in ΔH which lead to internal resonances [3,12]. An internal resonance can result in a significant energy exchange between the unperturbed modes. This assumption is valid for the magnetic field inhomogeneities considered here provided $\omega_{+0} \gg \omega_{z0} \gg \omega_{-0}$. From Eq, (13), the action variables J_j are approximate constants of motion for the perturbed problem and are related to the mode-amplitudes by

$$\begin{aligned} J_1 &= \tfrac{1}{2}m\omega_p R_+^2 \cong \tfrac{1}{2}qB_0R_+^2 \\ J_2 &= \tfrac{1}{2}m\omega_p R_-^2 \cong \tfrac{1}{2}qB_0R_-^2 \\ J_3 &= \tfrac{1}{2}m\omega_{z0}A_z^2 \end{aligned} \tag{14}$$

where we have used the approximation $\omega_p \approx \omega_c$ in the first two equations. From Eq. (13) the first-order frequency shifts are

$$\begin{aligned} \Delta\omega_+ &= \frac{\partial \langle \Delta H \rangle}{\partial J_1} \\ \Delta\omega_- &= \frac{-\partial \langle \Delta H \rangle}{\partial J_2} \\ \Delta\omega_z &= \frac{\partial \langle \Delta H \rangle}{\partial J_3} \end{aligned} \tag{15}$$

The observed frequencies for the perturbed motion are, therefore, $\omega_+ = \omega_{+0} + \Delta\omega_+$,

$w_- = \omega_{-0} + \Delta\omega_-$ and $\omega_z = \omega_{z0} + \Delta\omega_z$. To summarize, in order to calculate the frequency shifts by Eq. (15), one must derive $\Delta H(J_j, Q_j)$, then average ΔH over the angle variables to yield $\langle \Delta H \rangle$.

3. Results and discussion

3.1. Solenoidal magnetic field and vector potential

Solenoidal magnetic fields are the most important class of magnetic fields in ICR. Most ICR magnets, and to a lesser degree, the ICR trap and its support structure may all be considered as approximately axially symmetric. The non-cylindrically symmetric components of the magnetic field average out to zero over a period each of the ion's cyclotron, magnetron and z-oscillation modes of motion. Only inhomogeneous axially symmetric fields, which in addition possess symmetry under the operation $z \rightarrow -z$, can give mode-amplitude-dependent frequency shifts which are non-vanishing at first-order of perturbation theory. Furthermore, solenoidal magnetic fields greatly simplify the analysis since in this case only one component of the vector potential, A_θ, is non-zero in cylindrical coordinates. A well-known [15] pedagogical example of an axially symmetric magnetic field with reflection symmetry under the operation $z \rightarrow -z$ is the field of a tightly wound, finite length solenoid (see the appendix). Additional examples include a uniformly magnetized ring with magnetization direction parallel to the symmetry axis [7], and most electromagnets employed in ICR, NMR or ESR research.

For axially symmetric magnetic fields, it is possible to generate a power series expansion of the magnetic vector potential $\vec{A}$ at all points in space from just a knowledge of the magnetic field along the z-axis [16]. This result provides, in addition, a powerful method to extract the important solenoidal part of the magnetic field from experimental data of the on-axis magnetic field by fitting the on-axis field to a power series in z.

In this work, we assume that the magnetic field along the z-axis is adequately described by the three-term power series

$$B_z(\rho = 0, z) = B_0 + 2A_{20}z^2 + 8A_{40}z^4 + \ldots \tag{16}$$

where B_0 is the dominant homogeneous part of the magnetic field and A_{20} and A_{40} are expansion coefficients of the higher-order magnetic field [11]. The series expansion of A_θ is generated from $B_0(0, z)$ by application of the formula [16]

$$A_\theta(\rho, z) = \frac{\rho}{2}B_z(0, z) - \frac{1}{1!2!}\left(\frac{\rho}{2}\right)^3\frac{\partial^2 B_z(0, z)}{\partial z^2} + \left(\frac{1}{2!3!}\right)\left(\frac{\rho}{2}\right)^5\frac{\partial^4 B_z(0, z)}{\partial z^4} + \ldots \tag{17}$$

The first term on the right is just A_0 given by Eq. (3). With Eq. (16) substituted in Eq. (17) one obtains

$$A_\theta(\rho, z) = A_0 + \Delta A \tag{18}$$

where

$$\Delta A = A_{20}(\rho z^2 - \tfrac{1}{4}\rho^3) + A_{40}(4\rho z^4 - 6\rho^3 z^2 + \frac{1}{2}\rho^5) \tag{19}$$

The perturbation ΔA includes inhomogeneities due to both the radial and z-components of the magnetic field. The magnetic field $\vec{B} = B_z\hat{k} + B_\rho\hat{\rho} + B_\theta\hat{\theta} = \vec{\nabla} \times \vec{A}$ has z, radial and azimuthal components given by

$$B_z = \frac{1}{\rho}\frac{\partial}{\partial\rho}(\rho A_\theta) = B_0 + A_{20}(2z^2 - \rho^2) + A_{40}(8z^4 - 24\rho^2 z^2 + 3\rho^4)$$

$$B_\rho = -\frac{\partial A_\theta}{\partial z} = -2A_{20}\rho z + A_{40}(-16\rho z^3 + 12\rho^3 z)$$
$$B_\theta = 0 \qquad (20)$$

The magnetic field component B_z agrees with the orthogonal expansion of Laukien [11]. However, in our work no distinction between radial and axial components of the magnetic field is required since the vector potential automatically contains both magnetic field components. Since $\vec{\nabla}\cdot\vec{B} = 0$, a solenoidal magnetic field must in general contain both an axial and a radial magnetic field component.

3.2. Analytical frequency shifts

In order to evaluate the frequency shifts to the unperturbed eigenfrequencies by first-order perturbation theory, Eq. (15), one has to construct the perturbation Hamiltonian ΔH. The total Hamiltonian H is

$$H = \frac{1}{2m}[\vec{P} - q(\vec{A}_0 + \Delta\vec{A})]^2 + q\Phi_0 = H_0 + \Delta H \qquad (21)$$

H_0 is given by Eq. (2) and the perturbation is

$$\Delta H = -\frac{q}{m}\vec{P}\cdot\Delta\vec{A} + \frac{q^2}{m}\vec{A}_0\cdot\Delta\vec{A} + \frac{q^2}{2m}\Delta\vec{A}\cdot\Delta\vec{A} \qquad (22)$$

The third term on the right is second-order in ΔA and therefore is neglected. The magnitude of this term is usually much smaller than the first and second term on the right. The remaining terms yield

$$-\frac{q}{m}\vec{P}\cdot\Delta\vec{A} = -\frac{q}{m}L_z[A_{20}(z^2 - \tfrac{1}{4}\rho^2) + A_{40}(4z^4 - 6\rho^2 z^2 + \tfrac{1}{2}\rho^4)]$$
$$\frac{q^2}{m}\vec{A}_0\cdot\Delta\vec{A} = \frac{q^2 B_0}{2m}[A_{20}(\rho^2 z^2 - \tfrac{1}{4}\rho^4) + A_{40}(4\rho^2 z^4 - 6\rho^4 z^2 + \tfrac{1}{2}\rho^6)] \qquad (23)$$

where $L_z = xP_y - yP_x = J_2 - J_1$ is the z-component of angular momentum, which is a constant of motion for both the unperturbed as well as the perturbed ion motion. The Hamiltonian is also a constant of motion. The perturbation ΔH is transformed from cylindrical coordinates to action-angle variables by Eq. (9), then averaged over the angle variables to obtain $\langle\Delta H\rangle$. The necessary averages over the angle variables of ρ^{2n} and z^{2n} are evaluated using

$$z^2 = \frac{J_3}{m\omega_{z0}}(1 + \cos 2Q_3)$$
$$\rho^2 = \frac{2}{m\omega_p}[J_1 + J_2 + 2\sqrt{J_1 J_2}\cos(Q_1 + Q_2)] \qquad (24)$$

resulting in

$$\langle z^2\rangle = \frac{J_3}{m\omega_{z0}} \qquad \langle z^4\rangle = \frac{3J_3^2}{2m^2\omega_{z0}^2}$$
$$\langle\rho^2\rangle = \frac{2}{m\omega_p}(J_1 + J_2)$$
$$\langle\rho^4\rangle = \frac{4}{m^2\omega_p^2}(J_1^2 + J_2^2 + 4J_1J_2)$$
$$\langle\rho^6\rangle = \frac{8}{m^3\omega_p^3}(J_1^3 + J_2^3 + 9J_1J_2^2 + 9J_1^2J_2) \qquad (25)$$

With Eq. (24) substituted in Eq. (22) and using the approximation $\omega_p \approx \omega_c$ one obtains

$$\langle\Delta H\rangle = A_{20}\frac{q}{m}\left(\frac{2J_1J_3}{m\omega_{z0}} - \frac{J_1^2}{qB_0} - \frac{2J_1J_2}{qB_0}\right) + A_{40}\frac{q}{m}\left(\frac{12J_1J_3^2}{m^2\omega_{z0}^2} - \frac{24J_1^2J_3}{qB_0m\omega_{z0}} - \frac{48J_1J_2J_3}{qB_0m\omega_{z0}} + \frac{4J_1^3}{q^2B_0^2} + \frac{12J_1J_2^2}{q^2B_0^2} + \frac{24J_1^2J_2}{q^2B_0^2}\right) \qquad (26)$$

With Eq. (26) substituted in Eq. (15), then converting to amplitude variables by Eq. (14) yields the frequency shifts due to solenoidal magnetic field inhomogeneities. The final results are

$$\begin{aligned}\Delta\omega_+ &= A_{20}\frac{q}{m}(-R_+^2 - R_-^2 + A_z^2)\\ &\quad + A_{40}\frac{q}{m}(3A_z^4 - 12R_-^2A_z^2 - 12R_-^2A_z^2\\ &\quad + 3R_+^4 + 3R_-^4 + 12R_+^2R_-^2)\\ \Delta\omega_- &= A_{20}\frac{q}{m}R_+^2 + 6A_{40}\frac{q}{m}(2A_z^2 - R_-^2 - R_+^2)R_+^2\\ \Delta\omega_z &= A_{20}\frac{q}{m}\left(\frac{\omega_c}{\omega_{z0}}\right)R_+^2\\ &\quad + 6A_{40}\frac{q}{m}\left(\frac{\omega_c}{\omega_{z0}}\right)(A_z^2 - R_+^2 - 2R_-^2)R_+^2\end{aligned} \tag{27}$$

The frequency shifts to all three fundamental modes are dependent upon all three mode amplitudes. In agreement with Laukien [11], $\Delta\omega_+$ is inversely proportional to m/z, hence, $\Delta\omega_+/\omega_c$ is m/z independent. The magnetron and z-oscillation frequency shifts are predicted to vanish when the cyclotron radius is zero. This effect is understood by noting that the magnetic field perturbation is momentum dependent and since we have assumed $\omega_p \approx \omega_c$ which is valid when $\omega_{+0} \gg \omega_{z0} \gg \omega_{-0}$. For this situation, nearly all of the kinetic energy is contained in the cyclotron mode indicating that a small cyclotron radius or large m/z results in small frequency shifts. The z-oscillation frequency shift expression predicts that $\Delta\omega_z$ is in general much greater than the absolute shifts to $\Delta\omega_+$ and $\Delta\omega_-$ by a factor ω_c/ω_{z0}.

3.3. Numerical comparison

As an important test of the validity of the analytically derived frequency shifts Eq. (27) and to estimate the magnitude of the effect of various parameters involved, we have numerically integrated the exact equations of motion in amplitude-phase $(R_+, R_-, A_z; \beta_j)$ representation [12], to obtain the exact frequency shifts for some special cases. The perturbation force $\Delta\vec{F}$ used in the numerical ion trajectory calculations is given by $q\vec{v}\times\Delta\vec{B}$, where $\Delta\vec{B} = \vec{B} - \vec{B}_0$ and $\vec{v}$ is the ion velocity. The Cartesian coordinate components of $\Delta\vec{F}$ are

$$\begin{aligned}\Delta F_x &= q\left[v_y\Delta B_z - v_z B_\rho\left(\frac{y}{\rho}\right)\right]\\ \Delta F_y &= q\left[v_z B_\rho\left(\frac{x}{\rho}\right) - v_x\Delta B_z\right]\\ \Delta F_z &= q\left[v_x B_\rho\left(\frac{y}{\rho}\right) - v_y B_\rho\left(\frac{x}{\rho}\right)\right]\end{aligned} \tag{28}$$

where $\Delta B_z = B_z - B_0$, and B_z and B_ρ are given by Eq. (20). The exact equations of motion in amplitude-phase representation [12] are numerically integrated using the perturbation forces (Eq. (28)). The time derivative of the phases β_j are instantaneous frequency shifts and a slope of a straight line fit through the points β_j versus time yields the exact numerically evaluated frequency shift. Further details of this method are presented elsewhere [3,4,12].

The magnetic field parameters used in the numerical calculations are $B_0 = 4.7$ T, $A_{20} = -0.02$ T m^{-2} and $A_{40} = -24$ T m^{-4} which are typical magnitude values for a shimmed magnet taken from the work of Laukien [11]. Only the magnitudes of A_{20} and A_{40} were reported in Ref. [11]. While we have arbitrarily chosen their values as negative, we would like to point out that the coefficients A_{20} and A_{40} for an ideal finite length solenoid magnet are less than zero (see the appendix). We are mainly interested in typical magnitudes of the effects involved and in determining how well the analytical Eq. (27) and numerical results agree. In actual shimmed magnet systems, the signs of A_{20}

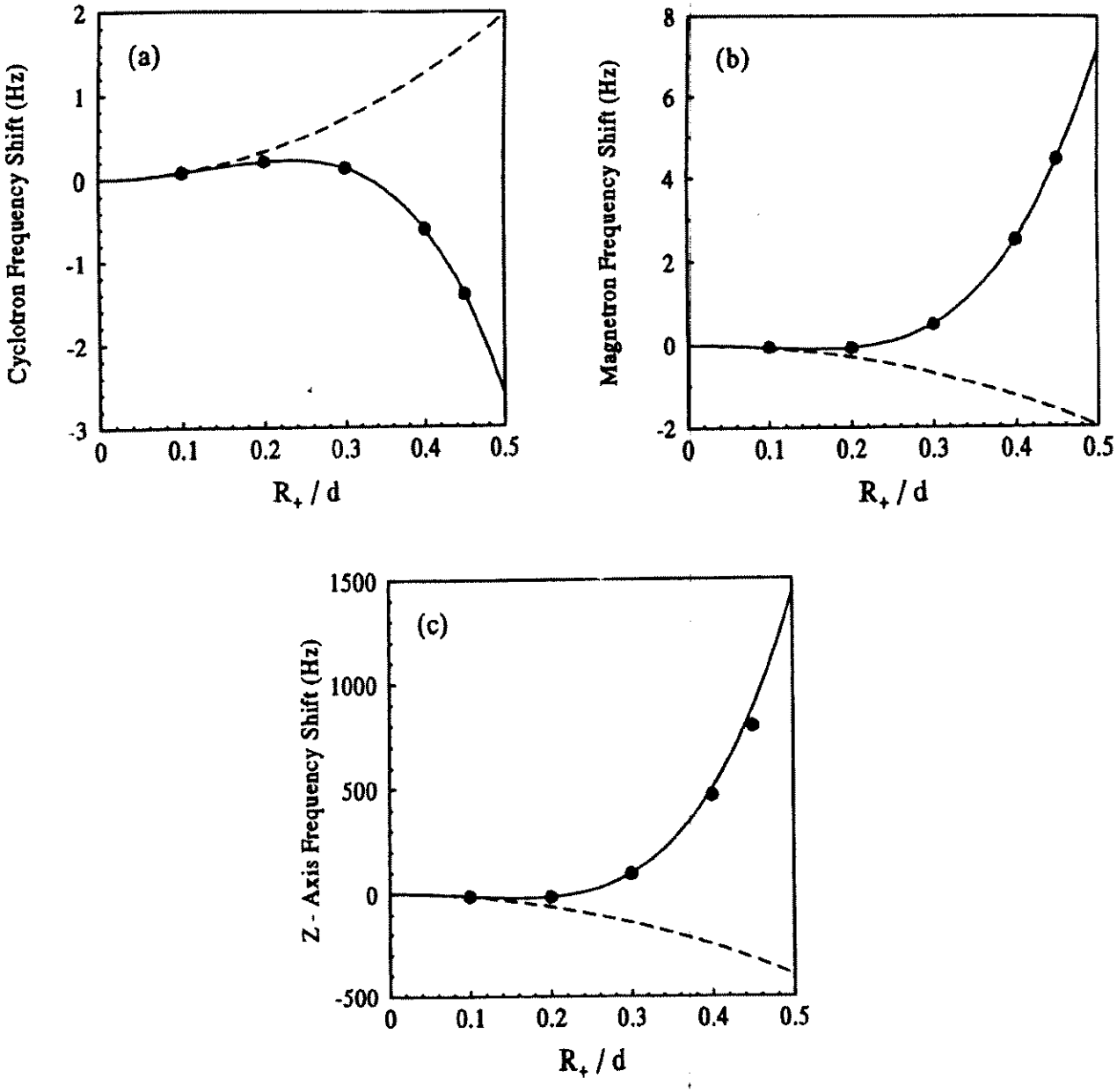

Fig. 1. Comparison of analytical (Eq. (27)) and exact numerical frequency shifts as a function of cyclotron radius when the magnetron radius and z-oscillation amplitude are zero ($R_- = A_z = 0$). The filled circles are calculated by numerical integration. Broken lines are results for only the second-order terms in Eq. (27) while the solid lines are the total of second- and fourth-order contributions. Parameters are $m/z = 100$ u, $q = e$, $V_t = 0.25$ V, $d = 0.0508$ m (cubic trap), $B_0 = 4.7$ T, $A_{20} = -0.02$ T m^{-2} and $A_{40} = -24$ T m^{-2}. (a) Cyclotron frequency shift, $\Delta\omega_+/2\pi$; (b) magnetron frequency shift, $\Delta\omega_-/2\pi$; (c) z-oscillation frequency shift, $\Delta\omega_z/2\pi$.

and A_{40} can be either positive or negative and should be measured in actual applications. Other parameters used in Eq. (27) and in the numerical simulations are $m/z = 100$ u, $q = e$, $V_t = 0.25$ V and $d = 0.0508$ m (cubic trap). The initial conditions include $R_- = 0$ (zero magnetron radius) and $\beta_j = 0$. For later comparison, the unperturbed frequencies ν_{+0}, ν_{-0} and ν_{z0} ($\omega_{j0} = 2\pi\nu_{j0}$) are 721 448.62 Hz, 9.09 Hz and 3622.30 Hz, respectively. Results of these numerical investigations are presented in Figs. 1 and 2 presented along with analytically derived frequency shifts.

Fig. 1 presents numerical and analytical

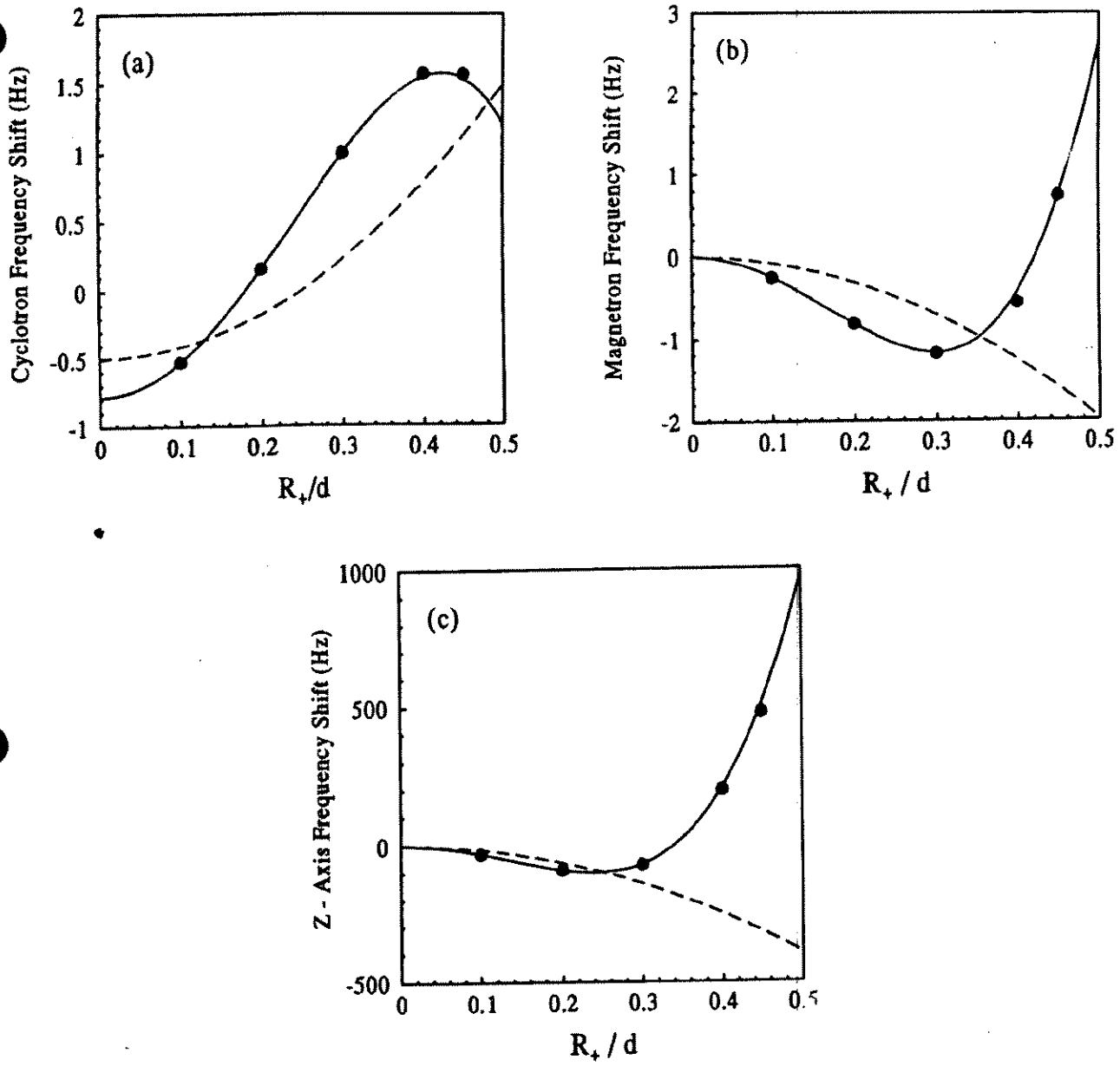

Fig. 2. Comparison of analytical (Eq. (27)) and exact numerical frequency shifts as a function of cyclotron radius for the case when the magnetron radius is zero ($R_- = 0$) and at the z-oscillation amplitude $A_z = 0.25d$. All other paramters are the same as in Fig. 1.

frequency shifts for the case when the cyclotron radius varies from zero to a maximum allowed radius of $R_+/d = 0.5$ at the trap boundary for the special case when both the magnetron radius R_- and z-oscillation amplitude A_z are zero. Exact numerical results are plotted as filled circles. The solid line corresponds to the sum of the second-order (proportional to A_{20}) and the fourth-order (proportional to A_{40}) contributions to the frequency shifts (Eq. (27)). The broken line is the frequency shift contribution from only the second-order contributions. Excellent agreement is found between the exact numerical and the analytical frequency shifts. One should also observe that for the values of A_{20} and A_{40} chosen, the fourth-order contribution to the frequency shift in all three modes is

non-negligible for $R_+ > 0.15d$. The fourth-order contribution dominates the second-order contribution for large cyclotron radii, therefore demonstrating the importance of including higher-order magnetic field terms in the calculation. Estimates of the relative shifts at $R_+ = 0.3d$ are $\Delta\omega_+/\omega_c \approx 0.2$ ppm, $\Delta\omega_z/\omega_z \approx 2.6\%$ and $\Delta\omega_-/\omega_- \approx 5.3\%$. For a cyclotron radius of $R_+ = 0.45d$, the relative shifts are $\Delta\omega_+/\omega_c \approx 2$ ppm, $\Delta\omega_z/\omega_z \approx 24\%$ and $\Delta\omega_-/\omega_- \approx 49\%$. Evidently large mode radii introduce relatively significant frequency shifts. In going from a cyclotron radius which is 60% of the maximum allowed radius to 90% of the maximum radius, the frequency shfit magnitude increase by an order of magnitude.

When $R_- = A_z = 0$, the numerical calculations corroborate the prediction that the frequency shifts are small when the cyclotron radius goes to zero. However, if the magnetron radius or z-oscillation amplitude is non-zero, then Eq. (27) predicts that $\Delta\omega_+ \neq 0$ in general, when the cyclotron radius is zero. These expectations are confirmed in Fig. 2(a). Fig. 2 presents results of analytically and numerically derived frequency shifts as a function of cyclotron radius for the case when the magnetron radius is zero, but the z-oscillation amplitude, $A_z = 0.25d$, is one-half of its maximum allowed value. As with Fig. 1, very good agreement is observed between numerically integrated and analytically derived frequency shifts for all three modes. An interesting result evident from the cyclotron frequency shifts given in Fig. 1(a) and 2(a) is their strong dependence on the z-oscillation amplitude. At relatively large cyclotron radii ($R_+ > 0.3$), the cyclotron frequency shift is negative when $A_z = 0$ and positive when $A_z = 0.25d$.

3.4. Modulation sidebands

Until now only the shifts to the unperturbed frequencies have been considered with no other consideration of the ion's trajectory. A Fourier series expansion of $\Delta H(J_j, Q_j)$ in the angle variables Q_j results in the angle-averaged perturbation, Eq. (26), which is independent of Q_j, as well as additional terms in the perturbation Hamiltonian which are dependent on Q_j. Phase terms are defined here as the Q_j dependent terms in this Fourier expansion. In this section we derive analytically in an approximate manner the corrections to the ion's trajectory due to the phase terms which have been averaged out in the frequency shift calculations. Previous numerical simulations [8] have demonstrated that in a strong magnetic bottle with $A_{20} \approx 50$–500 T m^{-2}, the Fourier transform of $x(t)$ results in not only a frequency component at ω_+, but also sidebands at $\omega_+ \pm 2\omega_z$ with relative amplitudes up to 10% of the fundamental. A strong magnetic bottle can be created, for example, by surrounding the ICR trap with a ring of ferromagnetic material [7]. In addition, numerical simulations [8] have demonstrated that only a single frequency at ω_z is observed in the spectrum for $z(t)$. The approach taken here is to approximately integrate the equations of motion and only average over the phase variables which do not significantly influence the ion motion when $\omega_{+0} \gg \omega_{z0} \gg \omega_{-0}$. All phase terms may lead to modulation effects but many give negligible contributions. The perturbation Hamiltonian before averaging gives for the second-order terms (neglecting the terms proportional to A_{40})

$$\Delta H = A_{20}\frac{q}{m}\left(\frac{2J_1J_3}{m\omega_{z0}} - \frac{2J_1J_2}{qB_0} - \frac{J_1^2}{qB_0} + \frac{2J_1J_3}{m\omega_{z0}}\cos 2Q_3\right) + \text{terms dependent on } \cos(Q_1 + Q_2) \text{ and } \cos(Q_1 + Q_2 \pm 2Q_3) \tag{29}$$

Upon integration of Hamilton's equations derived from Eq. (29), one can show that the

only non-negligible angle-variable-dependent term in Eq. (29) is $\cos 2Q_3$. Retaining only the terms in the bracket in Eq. (29) yields the equations of motion for J_j and Q_j.

$$\dot{J}_1 = \dot{J}_2 = 0 \qquad \dot{J}_3 = 2\Delta\omega_z J_3 \sin 2Q_3$$

$$\dot{Q}_1 = \omega_+ + 2A_{20}\frac{q}{m^2}\frac{J_3}{\omega_{z0}}\cos 2Q_3$$

$$\dot{Q}_2 = -\omega_-$$

$$\dot{Q}_3 = \omega_z + \Delta\omega_z \cos 2Q_3 \tag{30}$$

where $\omega_+ = \omega_{+0} + \Delta\omega_+$, $\omega_- = \omega_{-0} + \Delta\omega_-$ and $\omega_z = \omega_{z0} + \Delta\omega_z$ with the frequency shifts given by the second-order terms in Eq. (27). One should observe from Eq. (30) that the magnetron motion is unaffected by the phase terms. As seen in Eq. (29), the $\cos 2Q_3$ term only couples the z-mode with the cyclotron mode. These equations have an exact solution but are more easily integrated by successive approximations. For a first-order approximation in A_{20}, the J_j and Q_j terms on the right-hand sides of Eq. (30) are replaced by their unperturbed values (e.g. $J_3 \approx J_{30} =$ constant and $Q_3 \approx \omega_z t + \beta_{30}$ are used on the right). After integrating over time, then converting to amplitude-phase variables, the approximate x and z trajectory is found by Eqs. (6) and (7) then expanding to first-order in A_{20}. The z-position as a function of time is

$$z(t) \cong A_z\left(1 - \frac{\Delta\omega_z}{2\omega_{z0}}\right)\cos(\omega_z t + \beta_{30}) \tag{31}$$

where A_z and β_{30} are constants of motion determined from initial conditions. In agreement with numerical simulations [8] only a single frequency at ω_z is present to first-order in A_{20}. The x-position of the ion, neglecting magnetron motion, is given by

$$x(t) \cong R_+ \cos\left[\omega_+ t + \beta_{10} + \frac{A_{20}}{2B_0}\left(\frac{\omega_c}{\omega_{z0}}\right) \times A_z^2 \sin(2\omega_z t + 2\beta_{30})\right] \tag{32}$$

This result demonstrates that the cyclotron phase is modulated by a frequency at $2\omega_z$ which is not too surprising considering that the ion moves slowly along the z-axis compared to the cyclotron motion in a magnetic field which has even symmetry about the z-axis. Expanding $x(t)$ to first-order in A_{20} yields

$$x(t) \approx R_+ \cos(\omega_+ t + \beta_{10}) + R_+ \frac{A_{20}}{4B_0}\left(\frac{\omega_c}{\omega_{z0}}\right) A_z^2 \{\cos[(\omega_+ + 2\omega_z)t + \beta_{10} + 2\beta_{30}] - \cos[(\omega_+ - 2\omega_z)t + \beta_{10} - 2\beta_{30}]\} \tag{33}$$

Table 1
Magnetic susceptibilities χ and magnetizations M[a] (at an applied magnetic field of 47 kG) for some common ICR apparatus materials at temperatures T

Material	T (K)	χ CGS 10^{-6}	M[a] CGS
Cu	296	−0.77[b]	−0.04
Al	300	1.20[b]	0.06
Ti	293	14.4[b]	0.68
Ti	90	14.1[b]	0.66
Mo	298	9.48[b]	0.44
Mo	63.8	11.5[b]	0.54
Mo	20.4	15.9[b]	0.75
MACOR	4.2	13[c]	0.61
304 Stainless steel[d]	≈300	13000[e]	611
	≈300	640[f]	30

[a] $M = \chi B_0$, where $B_0 = 4.7$ T = 47 kG.
[b] From Ref. [18]; the χ value is converted from the molar susceptibilities χ_m listed in Ref. [18] by using $\chi = \chi_m(\rho/\mathrm{MW})$, where ρ and MW are the density and molecular weight, respectively.
[c] From Ref. [7].
[d] Two representative values of χ for stainless steel are listed. There is a wide range of χ values in the literature for this material.
[e] From Ref. [17]; $\chi(\mathrm{CGS}) = (4\pi)^{-1}\chi(\mathrm{MKS})$.
[f] From Ref. [19]; the relative permeability μ given in Ref. [19] is converted to χ by using the relation $\mu = 1 + 4\pi\chi$.

Therefore, three frequencies are present in the spectrum of $x(t)$: namely, a fundamental at ω_+ and sidebands at $\omega_+ \pm 2\omega_z$. The ratio R of the sideband amplitudes to the fundamental is

$$R = \left| \frac{A_{20}}{4B_0} \left(\frac{\omega_c}{\omega_{z0}} \right) A_z^2 \right| \tag{34}$$

with $B = 4.7$ T, $A_z = 0.25d$, $d = 0.0508$ m and $\omega_c/\omega_{z0} = 199$, corresponding to the same parameters used in the numerical simulations, $R \sim 0.002A_{20}$. With $A_{20} = 0.02$ T m^{-2}, the sidebands are negligible and $R \sim 0.004\%$; however with $A_{20} = 50$ T m^{-1} the sidebands are 10% of the fundamental amplitude. For typical well-shimmed ICR magnets, $|A_{20}| \sim 10^{-2}$ T m^{-2} the modulation sidebands are negligibly small.

3.5. Magnetization of the apparatus

It is interesting to inquire into the amount of magnetic field inhomogeneity introduced as a result of the magnetization of the materials comprising the ICR trap and its support structure due to the non-zero magnetic susceptibility in actual materials. Since the leading magnetic field inhomogeneity of a well-shimmed magnet has $|A_{20}| \sim 10^{-2}$ T m^{-2}, a relatively small value, it is important to determine the inhomogeneity arising from the apparatus. Russell and co-workers [17] have studied numerically the influence of magnetized ICR trap electrodes on ion injection into the trap and ion transfer in a dual cell, demonstrating the desirability of using low susceptibility materials such as Cu instead of stainless steel for the trap electrodes. We are interested here in determining the effect of the magnetized apparatus on A_{20} and higher-order coefficients.

In Table 1, we present a list of previously published values for magnetic susceptibility χ measured at temperature T. In addition, the magnetization (magnetic dipole moment per unit volume) M is given for an applied

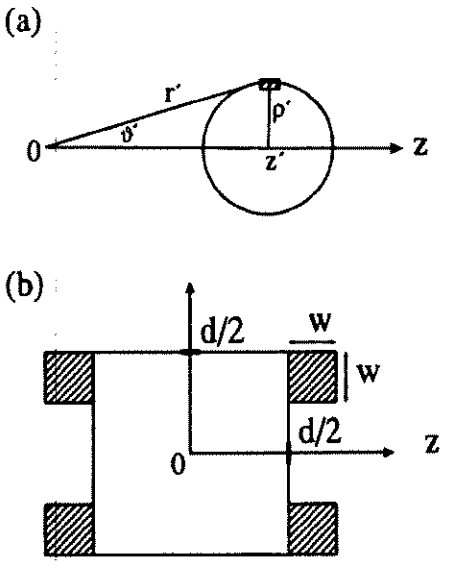

Fig. 3. (a) The geometry of a thin ring of magnetization located in the x–y plane and displaced along the z-axis. (b) A cross-section in the x–y plane of a cylindrical ICR trap whose length and diameter are d with insulator rings of cross-sectional area w^2 attached to the trapping plates.

external field of 4.7 T. While Cu and Al are relatively low susceptibility materials, stainless steel has a susceptibility three or four orders of magnitude greater.

The problem of the influence of the apparatus on the magnetic field inhomogeneity is a complicated one since the perturbed magnetic field depends on the amount and location of each type of material with presumably different magnetization. Hence, numerical rather than analytical approaches are the most amenable and one usually seeks solutions for specific geometries. Analytical results are possible for high symmetry geometries. Kretzschmar [13] has derived analytical frequency shifts for the case of a Penning trap whose hyperbolic electrodes are infinitely extended. This idealization may be appropriate to experiments employing small-dimensional Penning traps with massive electrodes; however, in most ICR experiments the traps have thin electrodes relative to the trap dimensions. Brown and Gabrielse [7] have derived the formula for the magnetic field of a thin ring of magnetized material whose

magnetization M is uniform and parallel to $\vec{B}_0$. The geometry is shown in Fig. 3(a). The ring of material lies in the x–y plane, centered on the z-axis but displaced from the origin along the z-axis a distance z'. The ring has a radius ρ' and cross-sectional area $d\rho'\,dz'$. The magnetic field perturbation due to a cylindrically symmetry apparatus aligned with $\vec{B}_0$ is calculated by integrating over all ring elements comprising the apparatus. The A_{20} coefficient obtained from the general expression of Brown and Gabrielse [7] is (in CGS units)

$$A_{20} = 12\pi \int \rho'\,d\rho'\,dz'\,M(\rho', z')\left(\frac{1}{r'}\right)^5 P_4(\cos\theta') \tag{35}$$

As indicated in Fig. 3(a), the ring element is located at ρ', z' in cylindrical coordinates or r', θ' in spherical coordinates, where r' is the distance to the ring from the origin and θ' is the polar angle. While Eq. (35) is formulated in CGS units, the CGS unit of A_{20} is equal to the MKS unit, namely 1 G cm^{-2} = 1 T m^{-2}. The A_{40} coefficient has an order of magnitude which is smaller than A_{20} by a factor $(r')^{-2}$, and can usually be neglected.

As a practical example in the application of Eq. (34), consider a cylindrical ICR trap of length d, diameter d, and wall thickness t ($t \ll d$), which is composed of a material with uniform magnetization M. Fig. 3(b) depicts the cross-section in the x–z plane of a cylindrical trap of length d and width d along with two insulating spacer rings (ex MACOR) of cross-sectional area w^2 located on the trap electrodes. Neglecting the spacer rings and just integrating Eq. (34) over the cylindrical trap yields

$$A_{20}(\text{trap}) \cong 12\sqrt{2}\pi M \frac{t}{d^3} \tag{36}$$

Eq. (36) is a specific result for a thinned-walled cylindrical trap whose length and diameter are equal. Assuming that the trap is made of Cu placed in a 4.7 T field gives $M(\text{Cu}) \approx -0.04$ (in CGS units). With $t = 0.16$ cm and $d = 5$ cm, one finds from Eq. (36) that $A_{20}(\text{trap}) = -0.003$ T m^{-2}. Using these same parameters except $d = 2.5$ cm, then $A_{20} = -0.02$ T m^{-2}. If the ICR trap is constructed from 304 stainless steel, then $A_{20}(\text{trap})$ increases by three to four orders of magnitude for the same thickness t. The use of a stainless steel trap may introduce (depending upon the trap dimension d and material thickness t employed) a magnetic field inhomogeneity several orders of magnitude greater than the intrinsic inhomogeneity of the ICR magnet.

The influence of the support structure on A_{20} should also be considered. We have numerically integrated Eq. (35), including the ceramic spacer rings, for the idealized situation depicted in Fig. 3(b). Using $d = 5$ cm and $w = 1.27$ cm yields $A_{20}(\text{spacer}) = -0.016M$. If the spacers are made of MACOR, then at $T = 4.2$ K and $B_0 = 4.7$ T, $M(\text{MACOR}) \cong +0.61$ (in CGS units) [7], yielding $A_{20} \cong -0.01$ T m^{-2}. However, at room temperature the magnitudes of the magnetic susceptibilities for MACOR and Cu are similar, and A_{20} with MACOR spacer rings would be reduced substantially.

From this example, it is clear that the magnetization of the apparatus can introduce a relatively substantial effect on the magnetic field inhomogeneity which can be larger than the inhomogeneity of the electromagnet. If high susceptibility materials or ferromagnetic impurities are present close to the ICR trap, then the homogeneity of the magnetic field may be greatly affected. In actual experiments, Eq. (35) should be integrated for the specific geometry employed since, as pointed out in earlier work [7,17], A_{20} is very sensitive to the location as well as the composition of the materials comprising the apparatus.

As a final example of the application of Eq. (35), we shall determine A_{20} as a function of

aspect ratio c/d, for a cylindrical ICR trap of length c and diameter d in the limit that the wall thickness t is much smaller than c and d. Neglecting the spacer rings and just integrating Eq. (34) over a thin walled cylindrical trap yields

$$A_{20}(\text{trap}) \cong -\frac{48\pi Mt}{d^3(1+\eta^2)^{7/2}} \times (1 - 3\eta - 4\eta^2 + 2\eta^3) \qquad (37)$$

where $\eta = c/d$ is the trap aspect ratio.

In the limit $c = d$ ($\eta = 1$), Eq. (37) reduces to Eq. (36). An important result from Eq. (37) is that A_{20}, due to magnetization of the cylindrical trap, can equal zero at special aspect ratio values. In particular, $A_{20}(\text{trap}) = 0$ when $c/d = 0.257$ and $c/d = 2.517$. For $0.257 < c/d < 2.517$, A_{20}/M is positive, otherwise A_{20}/M is negative. Additional flexibility in the choice of aspect ratio which tunes out A_{20} can be gained, for example, by allowing the trapping plates (end caps) to have a thickness different from that of the cylindrical ring electrode. In such situations it should be possible to tune out A_{20}, due to the magnetization of the apparatus, for an arbitrary trap aspect ratio by judicious choices of trapping plate and ring electrode thicknesses.

The magnetic field inhomogeneity due to the magnetization of the apparatus (i.e. the ICR trap and its support structure) is critically dependent on both the quantity and location of the material from the trap center. These characteristics are evident in Eq. (37) for the cylindrical ICR trap as a function of trap aspect ratio. The d^{-3} dependence of A_{20} indicates that the inhomogeneity decreases very rapidly with increasing trap diameter.

4. Conclusions

Solenoidal (i.e. axially symmetric) magnetic fields, which in addition possess symmetry under the operation $z \rightarrow -z$, are the most important to ion cyclotron mass spectrometry since they introduce frequency shifts at first-order in perturbation theory. Analyticaly frequency shifts (Eq. (27)) are derived by classical perturbation theory without any restriction on initial conditions, assuming $\omega_{+0} \gg \omega_{z0} \gg \omega_{-0}$, which is valid for most ICR experiments.

The frequency shifts (Eq. (27)) are dependent on all three fundamental mode amplitudes (i.e. the cyclotron radius, magnetron radius and the z-oscillation amplitude). The cyclotron and magnetron frequency shifts, to first-order, are inversely proportional to m/z and are directly proportional to the coefficients of the magnetic field inhomogeneity. The z-oscillation frequency shift is, in addition, proportional to the ratio ω_c/ω_{z0} and therefore is in general a much larger shift than the cyclotron and magnetron frequency shifts. The analytical results give very good agreement with frequency shifts obtained from numerical integration of the exact equations of motion.

The effect of the leading inhomogeneity (i.e. the magnetic bottle term) on the ion trajectory is investigated analytically, assuming $\omega_{+0} \gg \omega_{z0} \gg \omega_{-0}$. Even in a strong magnetic bottle, the z-trajectory (Eq. (31)) is a single frequency component at the shifted z-oscillation frequency. The z-amplitude is dependent on the magnetic bottle strength (A_{20}) and to the cyclotron radius. The magnetron trajectory is unaffected to first order in A_{20}, other than a frequency shift. On the other hand, the cyclotron motion (Eq. (32)) is frequency modulated at twice the z-oscillation frequency, resulting in a signal (Eq. (33)) which contains sidebands at $\omega_+ \pm 2\omega_z$ in addition to the fundamental at ω_+. The sidebands have amplitudes which are negligible for typical FT-ICR experiments but should be observable in experiments with intentionally strong magnetic bottle fields. The analytical results derived here are in agreement with results from previous [8] numerical trajectory calculations.

The magnetization of the ICR trap and its support structure. due to their being composed of materials with non-vanishing susceptibilities, introduces magnetic field inhomogeneities in addition to the intrinsic field from the external magnet. The important second-order coefficient A_{20} for a cylindrically symmetric apparatus is studied using the method of Brown and Gabrielse [7]. The value of A_{20} for a cylindrical ICR trap of length c, diameter d, wall thickness t and magnetization M, (where $t \ll c, d$) is given by Eq. (37). The magnetic bottle coefficient A_{20} is directly proportional to t and d^{-3} and can be tuned out at special aspect ratios.

Acknowledgments

We thank Dr. R. Chen and Dr. R.T. Kouzes for helpful discussions. This work was supported through the U.S. Department of Energy. Pacific Northwest Laboratory is operated by Battelle Memorial Institute through contract DE-AC06-76RLO 1830.

Appendix: On axis magnetic field of a finite length solenoid

Consider a tightly would solenoid of length L, radius a, N turns per meter, current I, origin at the center and aligned parallel to the z-axis. For this geometry the magnetic field along the z-axis is [15] (in MKS units)

$$B_z(0,z) = \frac{NI\mu_0}{2} \times \left[-\frac{\frac{L}{2}+z}{\sqrt{\left(\frac{L}{2}+z\right)^2+a^2}} + \frac{\frac{L}{2}-z}{\sqrt{\left(\frac{L}{2}-z\right)^2+a^2}} \right] \quad \text{(A1)}$$

Assuming that $z \ll L$ and $a \ll L$, then expanding (A1) in a Taylor series to terms up to $(a/L)^2$ and $(z/L)^6$ yields

$$B_z(0,z) \cong B_0 \left[\left(1 - 2\frac{a^2}{L^2}\right) - 24\frac{a^2}{L^4}z^2 - 160\frac{a^2}{L^6}z^4 - 896\frac{a^2}{L^8}z^6 - \ldots \right] \quad \text{(A2)}$$

where $B_0 = \mu_0 NI$ is the magnetic field of an infinitely long solenoid. The coefficients of the magnetic field inhomogeneity are found by comparison of Eq. (A2) with Eq. (16) resulting in

$$A_{20} = -12B_0\frac{a^2}{L^4} \qquad A_{40} = -20B_0\frac{a^2}{L^6}$$

References

[1] A.G. Marshall and F.R. Verdun, Fourier Transforms in NMR, Optical and Mass Spectrometry: A User's Handbook, Elsevier, Amsterdam, 1990.
[2] B. Asamoto (Ed.), FT-ICR/MS Analytical Applications of Fourier Transform Ion Cyclotron Resonance Mass Spectrometry, V.C.H., Weinheim, 1991.
[3] D.W. Mitchell, Int. J. Mass Spectrom. Ion Processes, in press.
[4] D.W. Mitchell, A.L. Rockwood, R. Chen and R.D. Smith, J. Chem. Phys., in press.
[5] A.L. Rockwood and M.G. Sherman, unpublished work.
[6] D.W. Mitchell, B.A. Hearn and S.E. DeLong, Int. J. Mass Spectrom. Ion Processes, 125 (1993) 95.
[7] L.S. Brown and G. Gabrielse, Rev. Mod. Phys., 58 (1986) 233.
[8] D.P. Weitekamp and P.J. Pizarro, Method and Apparatus for Highly Sensitive Spectroscopy of Trapped Ions, U.S. Patent 4 982 088, 1991.
[9] D. Schuch, K.-M. Chung and H. Hartmann, Int. J. Mass Spectrom. Ion Processes, 56 (1984) 109.
[10] H. Hartman and K.-M. Chung, Theor. Chim. Acta, 45 (1977) 137.
[11] F. Laukien, Int. J. Mass Spectrom. Ion Processes, 73 (1986) 81.
[12] D.W. Mitchell, Int. J. Mass Spectrom. Ion Processes, 107 (1991) 417.
[13] M. Kretzschmar, Z. Naturforsch. Teil A, 45 (1990) 965; Phys. Scr., 46 (1992) 544.
[14] M. Kretzschmar, Eur. J. Phys., 58 (1991) 240.

[15] J.D. Jackson, Classical Electrodynamics, Wiley, New York, 1975, p. 205.
[16] W.R. Smythe, Static and Dynamic Electricity, Hemisphere, New York, 1989, p. 288.
[17] E.L. Kerley, C.D. Hanson, M.E. Castro and D.H. Russell, Anal. Chem., 61 (1989) 2528.
[18] R.C. Weast (Ed.), Handbook of Chemistry and Physics, C.R.C. Press, Cleveland, OH, 1974, p. E120–E127.
[19] D. Peckner and I.M. Bernstein, Handbook of Stainless Steels, McGraw-Hill, New York, 1977, p. 19-3.